Effect of Temperature on Mechanical Performance and Tensoresistivity of a New Sensor-Enabled Geosynthetic Material

Xin-zhuang Cui[1]; Jun Li[2]; Jun-wei Su[3]; Qing Jin[4]; Yi-lin Wang[5]; and She-qiang Cui[6]

Abstract: In geotechnical engineering, geosynthetics are widely used as a reinforcement material for its numerous advantages. Moreover, its strain monitoring is increasingly crucial to ensure the safety of reinforced geotechnical structures. Therefore, a new sensor-enabled geosynthetic material named sensor-enabled geobelts (SEGB) was developed and manufactured. The SEGB has the reinforced function while achieving self-monitoring of strain. Its essence is a kind of conductive polymer, which is made from super conductive carbon black (CB) and high-density polyethylene (HDPE). To study the effects of temperature on the mechanical performance and the tensoresistivity of SEGB, two types of tensile tests were performed between its service temperature ranges (−20°C to 40°C). The results demonstrate that the tensile strength of SEGB first decreases with temperature and then becomes stable. However, the elongation at break consistently increases with the increase of the temperature. And the measurement results of the electrical resistance indicate the tensoresistivity response of SEGB become more sensitive with the temperature increases. Considering temperature effects, a nonlinear calibration model of the tensoresistivity was proposed to ensure the application of SEGB at different ambient temperatures. **DOI: 10.1061/(ASCE)MT.1943-5533.0002698.**

Author keywords: Sensor-enabled geobelts; Mechanical properties; Tensoresistivity; Temperature.

Introduction

Geosynthetics is a general term for synthetic materials used in the field of civil and geotechnical engineering (Wiewel and Lamoree 2016; Ingold 1994). It is made of synthetic polymers (e.g., plastics, chemical fiber, synthetic rubber) and is made into various types of products (e.g., geotextiles, geomembranes, geonets, fiberglass, geomats). These products are habitually placed inside the soil to enhance or protect the geotechnical structure (Koerner 2005). For instance, using geotextiles to handle the surface crackings of highway (Sudarsanan et al. 2018), using lightweight geosynthetics to deal with the settlements of embankment (Saride et al. 2015), using geocells to enhance the bearing capacities of foundation (Hegde 2017; Zhang et al. 2010), and using special geosynthetics to reinforce the paved roads (Liu et al. 2016).

In general, using geosynthetics as an effective tool to reinforce geotechnical structures is increasingly widespread. Subsequently, it becomes important to ensure the safety and health of the geosynthetic-reinforced structures via monitoring the strain of geosynthetics. The safety and health monitoring of geotechnical structures is a crucial task in the field of civil and geotechnical engineering. Therefore, a series of monitoring methods were proposed. The representatives are X-rays, digital imagery, fiber optic cables, and tomographic techniques (Kawaragi et al. 2009; Aydilek 2007; Zhao and Zhang 2009; Vangla and Gali 2014; Thomas and Cantre 2009; Zhang et al. 2014). However, due to the limitation of monitoring scope or accuracy, these methods cannot be effectively and efficiently applied on a large scale in the field. Therefore, it is hoped that the geosynthetics can be simultaneously given the functions of reinforcement and self-monitoring of strain, so that large-scale and efficient safety monitoring of geotechnical structures is available.

A new geosynthetic material called sensor-enabled geogrid (SEGG) was developed by Hatami et al. (Yazdani et al. 2015; Hatami et al. 2009). With a conductive coating, SEGG is able to reinforce the geotechnical structure while monitoring its strain. However, there are two main technical obstacles to SEGG. First, the waterproofing of SEGG has not been solved. Second, the conductive network formed by multiple ribs is too complicated, which may affect the accuracy of monitoring (Chen 2011). These mean the application of SEGG is confined to the laboratory, and cannot be used in the engineering field.

Therefore, the authors developed the sensor-enabled geobelt (SEGB), a new smart geosynthetic material, primarily made of super conductive carbon black (CB) and high-density polyethylene (HDPE) (Cui et al. 2018a, b; Li et al. 2018). SEGB was industrially manufactured. Moreover, it solved the problems that restricted the field application of SEGG and realized large-scale application in the engineering field.

The SEGB can be used in many situations of geotechnical and environmental engineering. And the temperature can be very different in these diverse service environments, engineering practices indicate that the temperature range in most situations is generally

[1]Professor, School of Civil Engineering, Shandong Univ., Jinan 250061, PR China (corresponding author). Email: cuixz@sdu.edu.cn

[2]Ph.D. Candidate, School of Civil Engineering, Shandong Univ., Jinan 250061, PR China. Email: forzaapis@126.com

[3]Graduate Student, School of Civil Engineering, Shandong Univ., Jinan 250061, PR China. Email: 1571201036@qq.com

[4]Lecturer, School of Civil Engineering, Shandong Univ., Jinan 250061, PR China. Email: 827762282@qq.com

[5]Ph.D. Candidate, School of Civil Engineering, Shandong Univ., Jinan 250061, PR China. Email: eason_wyl@163.com

[6]Graduate Student, School of Civil Engineering, Shandong Univ., Jinan 250061, PR China. Email: 1914569734@qq.com

Note. This manuscript was submitted on February 19, 2018; approved on November 15, 2018; published online on March 20, 2019. Discussion period open until August 20, 2019; separate discussions must be submitted for individual papers. This paper is part of the ***Journal of Materials in Civil Engineering***, © ASCE, ISSN 0899-1561.

between −20°C and 40°C (Soleimanbeigi et al. 2014; Osterkamp 1987; Luo et al. 2018; Christopher and Majid 2017). For instance, when this new smart geosynthetic material was applied in urban embankments or foundations, the temperature of the environment was high due to the thermal pipelines buried in the surrounding soil. A subzero situation often occurs in regions of high latitude and high altitude. Specifically, when laid in the permafrost, the SEGB needs to work at extremely low temperatures. Even if the SEGB is used in a usual foundation, the seasonal temperature variations can impact the strength, elongation, and electrical resistance of the SEGB. Therefore, the temperature effects on the mechanical performance and the tensoresistivity of the SEGB must be considered, especially between the service temperature ranges (−20°C to 40°C).

There have been no related studies of the mechanical properties and the tensoresistivity of sensor-enabled geosynthetics such as SEGB in this temperature range. Moreover, there have been no related studies of SEGBs as a type of conductive polymer, on its conductivity change involving tensile tests, especially the tensile tests between the temperature ranges of −20°C to 40°C. Most research on the temperature effects on conductive polymers has been focused on electrical properties, such as positive temperature coefficient (PTC) effects or tunneling effects, of the conductive polymers (Wan and Wen 2004; Bundur et al. 2017; Droval et al. 2008). There have been no adequate studies on the tensoresistivity of conductive polymers.

In this paper, to investigate the temperature effects on the mechanical performance and the tensoresistivity of the SEGB, a series of tensile tests was carried out within the temperature range of −20°C to 40°C. This study aims to calibrate the strain sensitivity of the electrical resistance of SEGB under different temperatures.

Fabrication and Features of SEGB

Materials and Fabrication of SEGB

SEGB was primarily made of two raw materials: One is high-density polyethylene (HDPE), which is the virgin polymer. The other is super conductive carbon black (CB), which is the conductive master batch. The basic parametric information of HDPE is provided in Table 1.

The industrial manufacture of SEGB is achieved by the twin-screw extruder. And its production process can be summarized as follows. According to the designed mass ratio, manually mix the CB master-batch and the HDPE master-batch to uniform. Then, respectively set the preheated temperatures of each working partition of the extruder to 180°C, 185°C, 190°C, 200°C, 213°C, and 205°C. When the temperature of the working partitions reaches the set temperature, the CB/HDPE mixture is fed into the extruder through the grape hopper so that the CB and HDPE are melting mixed via high temperature. Finally, the SEGB is molded and extruded. Note that the mixture must be kept as dry as possible throughout the whole production process.

Table 1. Basic parameters of HDPE

Parameter	Value
Tensile strength (Pa)	2.6×10^7
Elongation at break (%)	5.0×10^2
Density (g/cm^3)	9.5×10^{-3}

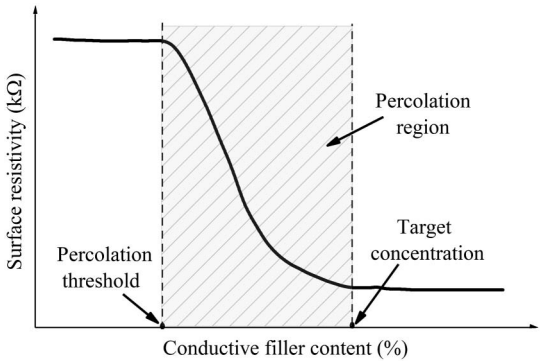

Fig. 1. Diagram of percolation theory of the conductive polymer.

Percolation Region and Optimal CB Content of SEGB

As the conductive filler, the content of CB has a significant effect on the electrical resistance of SEGB. Therefore, it is important to determinate the content of CB before the production of SEGB. In this study, the optimal content of CB was determined by the percolation theory. Fig. 1 shows the percolation phenomenon in a conductive polymer (Dong and Wang 2017; Peliskova et al. 2005). It is shown that with the increase in the conductive filler concentration, the electrical resistance remains stable at first. When the conductive filler exceeds a critical concentration, the electrical resistance drastically decreases until the conductive filler reaches the target concentration. Finally, the resistance tends to stabilize. The critical concentration of the conductive filler is called the percolation threshold, and the target concentration is the optimal content of the conductive filler.

Fig. 2 demonstrates the change in the surface resistivity of SEGB with its CB concentration. It is shown that once the CB concentration exceeds the percolation threshold, the surface resistivity gradually decreases as the CB concentration continues to increase. According to the percolation theory, the growth of CB concentration changes the distribution state of CB in the conductive polymer, gradually forming a CB-conductive network. And the electrons can be transported across the polymer barriers via the CB-conductive network, thereby reducing the surface resistivity of SEGB (Yazdani et al. 2015; Huang 2002). However, when the CB concentration reaches the target concentration 47.5%, the optimal CB concentration, the surface resistivity begins to stabilize and does not continue to decrease. It indicates that the final structure of the CB-conductive network has been formed. Thereafter, the growth of CB concentration can no longer change the state of the CB-conductive network.

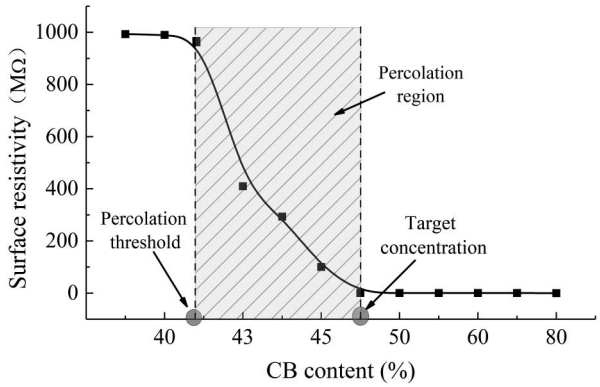

Fig. 2. Diagram of the percolation region of SEGB.

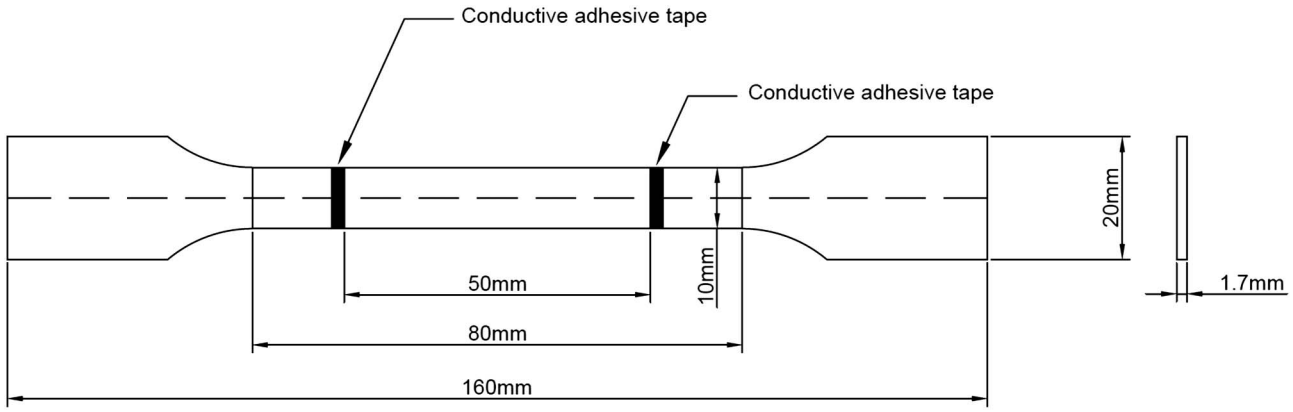

Fig. 3. Dimensions of SEGB specimen used in the fast/slow tensile tests.

And thereafter, if the CB-conductive network structure is damaged, the conductivity of the SEGB can respond.

Mechanical Properties of SEGB

The tensile strength and the elongation at break are significant indicators that reflect the tensile properties of the SEGB, and they are the basis for evaluating the reinforcement performance of the SEGB. These two indicators can be obtained via the fast tensile tests. The SEGB specimen used in the fast tensile tests is shown in Fig. 3. And the whole process can be described as follows. First, the specimen was installed on the universal testing machine. Then the tensile loading speed was set to 20 mm/min according to the Plastics-Determination of Tensile Properties (AQSIQ 2006). Finally, the machine was start until the specimen is damaged. And all the experimental data was automatically recorded by the machine. A typical stress-strain curve of SEGB obtained via the fast tensile tests is shown in Fig. 4.

Tensoresistivity of SEGB

The SEGB is essentially a kind of conductive polymer. It has a special property that its electric resistance can regularly change with strain, which is the core principle of SEGB to achieve self-monitoring of strain. The term tensoresistivity defines this property, which reflects the sensitivity of conductivity to the strain.

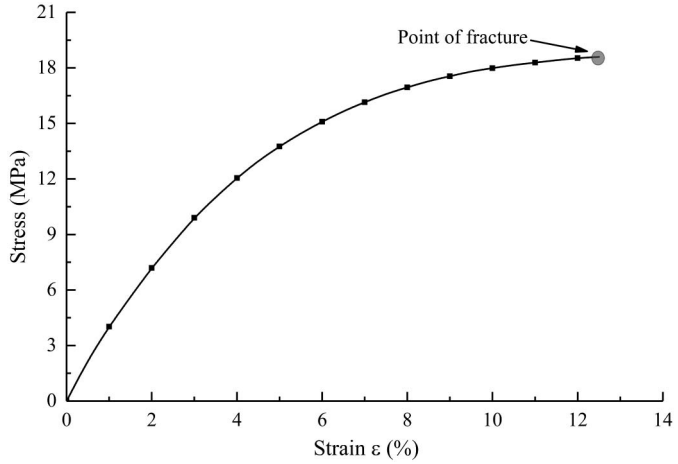

Fig. 4. Typical stress–strain curve of SEGB.

The analysis of tensoresistivity requires the slow tensile tests. The SEGB specimen used in the slow tensile tests is demonstrated in Fig. 3. Its dimensions are the same as those used in the fast tensile tests. Similarly, the slow tensile tests were carried out on the universal test machine. However, the loading mode of the slow tensile tests is different and it can be described as follows.

One loading cycle was a total of 4 min. Within the first minute, the tensile loading speed was set to 0.25 mm/min. Within the following 3 min, the tensile loading speed was adjusted to 0.001 mm/min to simulate the static state. Then this loading cycle was repeated until the strain reach to 10%. During the test, the surface resistance R_s was recorded at the end of each cycle. For the convenience of analysis, the surface resistance was normalized as follows:

$$k = \frac{R_s}{R_o} \tag{1}$$

where k = normalized resistance; R_o = original surface resistance (MΩ); and R_s = surface resistance during the test (MΩ).

A typical normalized resistance curve of SEGB obtained via the slow tensile tests is shown in Fig. 5.

Control of Ambient Temperature

To investigate the effects of temperature on the mechanical performance and tensoresistivity of SEGB under different temperatures, a temperature control system was assembled and added onto the universal testing machine. The system can provide a temperature range from −30°C to 120°C. After the temperature reached the target temperature for the test, the temperature was maintained for 20 min,

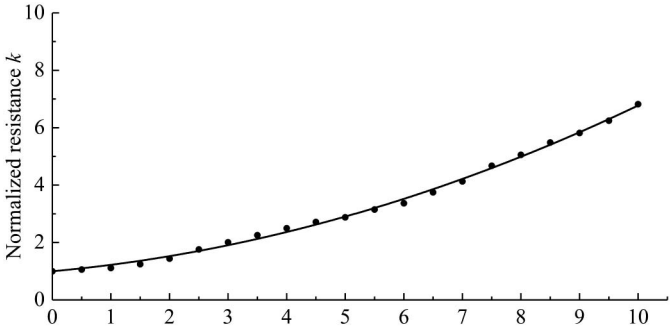

Fig. 5. Typical normalized resistance curve of SEGB.

Fig. 6. Setup diagram of the tensile test at different temperatures: (a) SEGB specimen waiting for test; (b) temperature control system; (c) SEGB specimen installation; and (d) SEGB specimen at −10°C.

and then the fast and slow tensile tests were performed. The temperatures controlled in the tests were from −20°C to 40°C in 5°C intervals for a total of 13 tests. Fig. 6 shows the setting up diagram of the slow/fast tensile test at the different temperatures.

Results and Discussions

Mechanical Properties of SEGB at the Different Temperatures

Table 2 shows the tensile strength and elongation at break of SEGB at the different temperatures in the fast test. In order to more obviously reveal the changes of tensile strength at different temperatures, a ratio of tensile strength is defined as

$$R_t = \frac{\sigma_u}{\sigma_{25}} \tag{2}$$

where R_t = ratio of tensile strength; σ_u = tensile strength of SEGB (MPa); and σ_{25} = tensile strength at 25°C (MPa).

Analogously, a ratio of elongation at break is defined as

$$R_e = \frac{E_u}{E_{25}} \tag{3}$$

where R_e = ratio of elongation at break; E_u = elongation at break of SEGB; and E_{25} = elongation at break at 25°C.

Table 2. Tensile strength and elongation at break in the fast test

Temperature (°C)	Tensile strength (MPa)	Elongation at break (%)
−20	28.83799	8.16863
−15	27.27619	9.00090
−10	23.68084	8.23695
−5	19.87618	8.10300
0	16.89261	10.67217
5	12.17265	12.60156
10	11.24681	12.55769
15	10.85320	18.63143
20	10.64449	29.66825
25	10.42165	29.16059
30	11.21332	35.14102
35	11.20474	38.69881
40	11.46929	41.29270

Fig. 7 shows the variations of R_t and R_e of SEGB with temperature. The tensile strength within the range of 10°C to 40°C does not change much. When the temperature is less than 10°C, the tensile strength sharply increases with the decrease in temperature. At −20°C the ratio of tensile strength reaches the maximum of 2.77. Meanwhile, the elongation at break shows a fairly slow increasing trend and remains at quite a low level, within the range of −20°C to 10°C, almost under 0.5. When the temperature is above 10°C, the elongation at break rapidly rises with the growth of temperature. At 40°C, the ratio of elongation at break reaches the maximum of 1.41.

From the microperspective, when the temperature is within the range of 10°C to 40°C, the molecular chains of the HDPE have better flexibility compared with that within the range of −20°C to 10°C. This flexibility allows the molecular chains to extend more easily when they are stretched (Shimada and Szwarc 1975), and the flexibility increases with temperature. Therefore, the elongation at break presents a rapidly increasing trend from 10°C to 40°C. Meanwhile, the interactive forces between the molecules do not change much. Thus, the tensile strength tends to be stability within this temperature range. When the temperature is less than 10°C, especially less than 0°C, the interactive force between the molecules increases as the temperature decreases because of the reduction in the molecular kinetic energy (Patra and Yethiraj 2000; Yamashiro et al. 2007). Therefore, the tensile strength sharply increases with the decrease in temperature. However, within this temperature range, the flexibility of the molecular chains sharply decreases

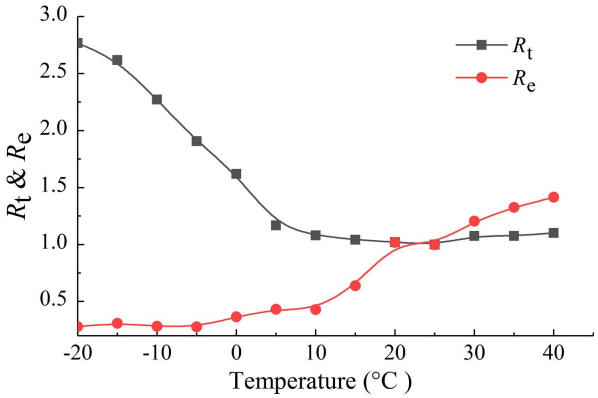

Fig. 7. Variation curves of R_t and R_e with temperature in the fast test.

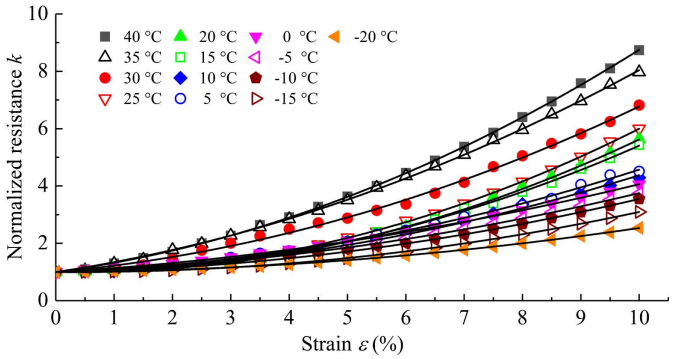

Fig. 8. Variation curves of normalized resistance at different temperatures.

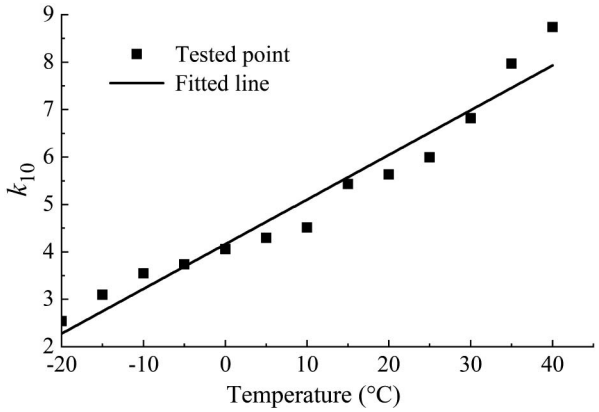

Fig. 10. Variation curves of k_{10} with temperature.

so that the elongation at break decreases to a lower level and shows a slow increase trend with the temperature increase.

Tensoresistivity of SEGB at the Different Temperatures

The variation trends of the normalized resistance with the strain of the SEGB at different temperatures are demonstrated in Fig. 8. The results show remarkably consistent variation trends. In the initial phase, the normalized resistance grows very slowly. Subsequently, its increasing rate is significantly improved. Fig. 8 also shows that the strain sensitivity of the electrical resistance rises with temperature. This result means that as the temperature rises, the electrical resistance can increase between the temperature ranges of −20°C to 40°C. And as shown in Fig. 8, the variation trends of the normalized resistance with strain can be fitted via a series of quadratic polynomial functions, which supports the previous research results of the authors (Cui et al. 2018a, b; Li et al. 2018).

It can be seen that all the curves in Fig. 8 demonstrated significant similarities. Therefore, as shown in Fig. 9, a ratio can be defined as the normalized resistance k divided by the normalized resistance k_{10} to eliminate the effects of temperature, where the k_{10} is the normalized resistance corresponding to the strain of 10%. It is shown in Fig. 9 that the variation of k/k_{10} is basically independent of the temperature. Moreover, the variation trend can be fitted via the following quadratic polynomial function:

$$\frac{k}{k_{10}} = a\varepsilon^2 + b\varepsilon + c \quad r = 0.99 \tag{4}$$

where the fitting parameters $a = 0.01623$, $b = 0.00688$, and $c = 0.15004$; and r = correlation coefficient.

In Eq. (4), k_{10} is related to temperature, and the variation trend of k_{10} with temperature is demonstrated in Fig. 10. It can be seen that the k_{10} increases with the temperature increase. Moreover, there is nearly a linear increase for k_{10} with temperature. This result indicates that the damage to the structure of CB conductive networks induced by the tensile strain demonstrates a gradual increasing trend with the increase of temperature. Moreover, the further damage to the CB conductive networks triggers a continuous increase in normalized resistances. Therefore, within the service temperature range, the electrical conductivity response of the SEGB becomes more sensitive as the temperature increases. Using the linear regression analysis method, the relationship between k_{10} and the temperature can be established

$$k_{10} = 0.09421T + 4.163(-20°\text{C} \le T \le 40°\text{C}) \quad r = 0.96 \tag{5}$$

where k_{10} = normalized resistance of SEGB when the strain is 10%; and T = temperature; and r = correlation coefficient.

Form Eqs. (4) and (5), a nonlinear calibration model of the tensoresistivity was proposed within the temperature range of −20°C to 40°C

$$k = (0.09421T + 4.163)(0.01623\varepsilon^2 + 0.00688\varepsilon + 0.15004) \tag{6}$$

It can be seen that the variables in Eq. (6) include both temperature and strain.

The Eq. (6) is a uniform model, and it can be seen that the independent variables in Eq. (6) include both temperature and strain. It means this uniform model can reflect the effects of temperature and strain on the normalized resistance of SEGB. And as shown in Fig. 11, the fitted values have a high consistency with the experimental values.

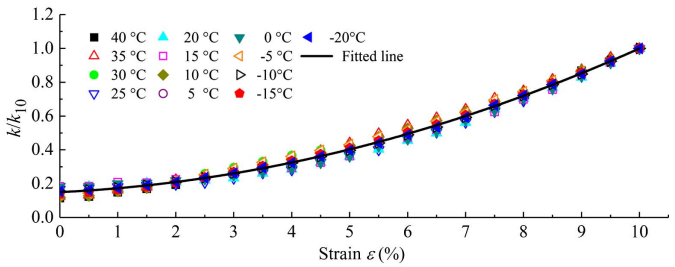

Fig. 9. k/k_{10} curve of the normalized resistance.

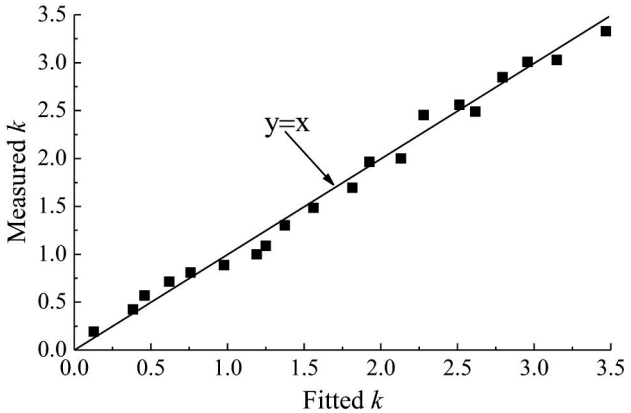

Fig. 11. Fitting effect of the uniform model.

Conclusions

In this study, the effects of temperature on the mechanical performance and tensoresistivity of SEGB were investigated. Based on the tests at different temperatures, a uniform tensoresistivity model of SEGB was proposed. The following conclusions were drawn:

- The tensile strength of SEGB did not change much and showed a good stability within the temperature range of 10°C to 40°C, while from 10°C to −20°C, the tensile strength increased rapidly with the decrease in temperature.
- Taking 10°C as a temperature dividing point, below 10°C, the elongation at break of SEGB stayed at a low level and presented a slowly increasing trend with the increase in temperature. When the temperature was above 10°C, the elongation at break showed a rapid increasing trend with the increase in temperature.
- The change in the normalized resistance with the strain of SEGB at different temperatures showed a similar trend. In the initial phase, the normalized resistance grows very slowly. Subsequently, its increasing rate is significantly improved. And the higher the temperature was, the better the tensoresistivity of SEGB.
- Considering the influences of both temperature and strain, a nonlinear model $[k = (0.09421T + 4.163)(0.01623\varepsilon^2 + 0.00688\varepsilon + 0.15004)$ Eq. (6)] was used to unify all the normalized resistance-strain curves within the service temperature range. This uniform model can be used to calibrate the tensoresistivity and to ensure the application of SEGB at different ambient temperatures.

Acknowledgments

The authors are grateful to the support of the National Key Research and Development Project (2018YFB1600100), Natural Science Foundations of China (51778346, 51479105), and Shandong Key R. & D. Project (2017GGX50102).

References

AQSIQ (Administration of Quality Supervision, Inspection and Quarantine). 2006. *Plastics—Determination of tensile properties*. GB/T 1040.1. Beijing: Standards Press of China.

Aydilek, A. H. 2007. "Digital image analysis in geotechnical engineering education." *J. Prof. Issues Eng. Educ. Pract.* 133 (1): 38–42. https://doi.org/10.1061/(ASCE)1052-3928(2007)133:1(38).

Bundur, Z. B., S. Bae, M. J. Kirisits, and R. D. Ferron. 2017. "Biomineralization in self-healing cement-based materials: Investigating the temporal evolution of microbial metabolic state and material porosity." *J. Mater. Civ. Eng.* 29 (8): 04017079. https://doi.org/10.1061/(ASCE)MT.1943-5533.0001838.

Chen, Q. 2011. "Discussion of 'Sensor-enabled geosynthetics: Use of conducting carbon networks as geosynthetic sensors' by Kianoosh Hatami, Brian P. Grady, and Matthew C. Ulmer." *J. Geotech. Geoenviron. Eng.* 137 (4): 435–436. https://doi.org/10.1061/(ASCE)GT.1943-5606.0000304.

Christopher, L. M., and T. Majid. 2017. "A method for correcting field strain measurements to account for temperature effects." *Geotext. Geomembr.* 45 (4): 250–260. https://doi.org/10.1016/j.geotexmem.2017.02.005.

Cui, X. Z., S. Q. Cui, Q. Jin, Y. L. Wang, L. Zhang, and Z. X. Wang. 2018a. "Laboratory tests on the engineering properties of sensor-enabled geobelts (SEGB)." *Geotext. Geomembr.* 46 (1): 66–76. https://doi.org/10.1016/j.geotexmem.2017.10.004.

Cui, X. Z., S. Q. Cui, T. Lu, L. Zhang, Y. L. Wang, and J. Li. 2018b. "Evaluation of the performance of sensor-enabled geobelts after cyclic loading." *Constr. Build. Mater.* 185 (Oct): 414–422. https://doi.org/10.1016/j.conbuildmat.2018.07.046.

Dong, S., and X. J. Wang. 2017. "Alignment of carbon iron into polydimethylsiloxane to create conductive composite with low percolation threshold and high piezoresistivity: Experiment and simulation." *Smart Mater. Struct.* 26 (4): 1–11. https://doi.org/10.1088/1361-665X/aa62d2.

Droval, G., J. F. Feller, P. Salagnac, and P. Glouannec. 2008. "Conductive polymer composites with double percolated architecture of carbon nanoparticles and ceramic microparticles for high heat dissipation and sharp PTC switching." *Smart Mater. Struct.* 17 (2): 1–10. https://doi.org/10.1088/0964-1726/17/2/025011.

Hatami, K., B. P. Grady, and M. C. Ulmer. 2009. "Sensor-enabled geosynthetics: Use of conducting carbon networks as geosynthetic sensors." *J. Geotech. Geoenviron. Eng.* 135 (7): 863–874. https://doi.org/10.1061/(ASCE)GT.1943-5606.0000062.

Hegde, A. 2017. "Geocell reinforced foundation beds past findings, present trends and future prospects: A state of the art review." *Constr. Build. Mater.* 154 (Nov): 658–674. https://doi.org/10.1016/j.conbuildmat.2017.07.230.

Huang, J. C. 2002. "Carbon black filled conducting polymers and polymer blends." *Adv. Polym. Tech.* 21 (4): 299–313. https://doi.org/10.1002/adv.10025.

Ingold, T. S. 1994. "Introduction." Chap. 1 in *Geotextiles and geomembranes handbook*, 1–70. Oxford, UK: Elsevier.

Kawaragi, C., T. Yoneda, T. Sato, and K. Kaneko. 2009. "Microstructure of saturated bentonites characterized by X-ray CT observations." *Eng. Geol.* 106 (1): 51–57. https://doi.org/10.1016/j.enggeo.2009.02.013.

Koerner, R. M. 2005. "Overview of geosynthetics." Chap. 1 in *Designing with geosynthetics*, 1–78. Upper Saddle River, NJ: Prentice-Hall.

Li, J., X. Z. Cui, Q. Jin, J. W. Su, S. Q. Cui, and Y. L. Wang. 2018. "Laboratory investigation of the durability of a new smart geosynthetic material." *Constr. Build. Mater.* 169 (Apr): 28–33. https://doi.org/10.1016/j.conbuildmat.2018.02.187.

Liu, L., Z. H. Liu, J. Y. Liu, and S. Li. 2016. "Fatigue performance of interlaminar anticracking material for rigid-flexible composite pavement." *J. Mater. Civ. Eng.* 28 (10): 06016012. https://doi.org/10.1061/(ASCE)MT.1943-5533.0001631.

Luo, D. L., H. J. Jin, Q. B. Wu, V. F. Bense, R. He, Q. Ma, S. H. Gao, X. Y. Jin, and L. A. Lu. 2018. "Thermal regime of warm-dry permafrost in relation to ground surface temperature in the source areas of the Yangtze and Yellow rivers on the Qinghai-Tibet plateau, SW China." *Sci. Total Environ.* 618 (Mar): 1033–1045. https://doi.org/10.1016/j.scitotenv.2017.09.083.

Osterkamp, T. E. 1987. "Permafrost temperatures in the Arctic national wildlife refuge." *Cold Reg. Sci. Technol.* 15 (2): 191–193. https://doi.org/10.1016/0165-232X(88)90064-X.

Patra, C. N., and A. Yethiraj. 2000. "Generalized van der Waals density functional theory for nonuniform polymers." *J. Chem. Phys.* 112 (3): 1579–1584. https://doi.org/10.1063/1.480706.

Peliskova, M., J. Vilcakova, M. Omastova, P. Saha, C. Z. Li, and O. Quadrat. 2005. "The effect of pressure deformation on dielectric and conducting properties of silicone rubber polypyrrole composites in the percolation threshold region." *Smart Mater. Struct.* 14 (5): 949–952. https://doi.org/10.1088/0964-1726/14/5/032.

Saride, S., A. J. Puppala, R. Williammee, and S. K. Sirigiripet. 2015. "Use of lightweight ECS as a fill material to control approach embankment settlements." *J. Mater. Civ. Eng.* 22 (6): 607–617. https://doi.org/10.1061/(ASCE)MT.1943-5533.0000060.

Shimada, K., and M. Szwarc. 1975. "Flexibility of molecular chains studied by electron-spin resonance technique." *J. Am. Chem. Soc.* 97 (12): 3313–3321. https://doi.org/10.1021/ja00845a006.

Soleimanbeigi, A., T. B. Edil, D. M. Asce, C. H. Benson, and F. Asce. 2014. "Effect of temperature on geotechnical properties of recycled asphalt shingle mixtures." *J. Geotech. Geoenviron. Eng.* 141 (2): 1–14. https://doi.org/10.1061/(ASCE)GT.1943-5606.0001216.

Sudarsanan, N., S. R. Mohapatra, R. Karpurapu, and V. Amirthalingam. 2018. "Use of natural geotextiles to retard reflection cracking in highway pavements." *J. Mater. Civ. Eng.* 30 (4): 04018036. https://doi.org/10.1061/(ASCE)MT.1943-5533.0002195.

Thomas, H., and S. Cantre. 2009. "Applications of low-budget photogrammetry in the geotechnical laboratory." *Photogramm. Rec.* 24 (128): 332–350. https://doi.org/10.1111/j.1477-9730.2009.00551.x.

Vangla, P., and M. L. Gali. 2014. "Image-segmentation technique to analyze deformation profiles in different direct shear tests." *Geotech. Test. J.* 37 (5): 828–839. https://doi.org/10.1520/GTJ20130138.

Wan, Y., and D. J. Wen. 2004. "Thermo-sensitive properties of carbon-black-loaded styrene butadiene rubber composite membranes." *Smart Mater. Struct.* 13 (5): 983–989. https://doi.org/10.1088/0964-1726/13/5/002.

Wiewel, B. V., and M. Lamoree. 2016. "Geotextile composition, application and ecotoxicology—A review." *J. Hazard. Mater.* 317 (Nov): 640–655. https://doi.org/10.1016/j.jhazmat.2016.04.060.

Yamashiro, M., H. Yamada, and S. Hamaguchi. 2007. "Molecular dynamics simulations of organic polymer dry etching at high substrate temperatures." *Jpn. J. Appl. Phys. Part 1* 46 (4A): 1692–1699. https://doi.org/10.1143/JJAP.46.1692.

Yazdani, H., K. Hatami, and B. P. Grady. 2015. "Sensor-enabled geogrids for performance monitoring of reinforced soil structures." *J. Test. Eval.* 44 (1): 391–401. https://doi.org/10.1007/s40891-016-0077-z.

Zhang, L., M. Zhao, C. Shi, and H. Zhao. 2010. "Bearing capacity of geocell reinforcement in embankment engineering." *Geotext. Geomembr.* 28 (5): 475–482. https://doi.org/10.1016/j.geotexmem.2009.12.011.

Zhang, Z., H. Yang, and H. Luo. 2014. "A novel fiber optic geophone with high sensitivity for geo-acoustic detection." *Int. Symp. Optoelectron. Technol. Appl.* 9297 (31): 1–7. https://doi.org/10.1117/12.2072653.

Zhao, Z. Y., and Q. Y. Zhang. 2009. "Digital photography monitoring in three-dimensional model experiment of deformation on water conservancy project." *Water Res. Power* 27 (5): 69–71.